Eulerian laser Doppler vibrometry: Online blade damage identification on a multi-blade test rotor

A.J. Oberholster, P.S. Heyns*

Dynamic Systems Group, Department of Mechanical and Aeronautical Engineering, University of Pretoria, Pretoria 0002, South Africa

Abstract

Laser Doppler vibrometry enables the telemetry-free measurement of online turbomachinery blade vibration. Specifically, the Eulerian or fixed reference frame implementation of laser vibrometry provides a practical solution to the condition monitoring of rotating blades. The short data samples that are characteristic of this measurement approach do however negate the use of traditional frequency domain signal processing techniques. It is therefore necessary to employ techniques such as time domain analysis and non-harmonic Fourier analysis to obtain useful information from the blade vibration signatures. The latter analysis technique allows the calculation of phase angle trends which can be used as indicators of blade health deterioration, as has been shown in previous work for a single-blade rotor.

This article presents the results from tests conducted on a five-blade axial-flow test rotor at different rotor speeds and measurement positions. With the aid of artificial neural networks, it is demonstrated that the parameters obtained from

* Corresponding author. Tel.: +2712 420 2432; fax: +2712 362 5087;

e-mail address: stephan.heyns@up.ac.za

non-harmonic Fourier analysis and time domain signal processing on Eulerian laser Doppler vibrometry signals can successfully be used to identify and quantify blade damage from among healthy blades. It is also shown that the natural frequencies of individual blades can be approximated from the Eulerian signatures recorded during rotor run-up and run-down.

Keywords

Online blade condition monitoring, Eulerian laser Doppler vibrometry, Multi-blade rotor, Non-harmonic Fourier analysis, Time domain analysis, Artificial neural networks

1. Introduction

Laser Doppler vibrometry allows the measurement of vibration on rotating blades in a non-contact fashion, thus eliminating the need for telemetry. Blade vibration data can be measured in a rotating (i.e. Lagrangian) reference frame or a stationary (i.e. Eulerian) reference frame. The first approach is better known as tracking laser Doppler vibrometry (TLDV) and involves controlling the laser beam orientation in order to follow a specific point on a blade during rotation. This technique requires line-of-sight with the blade over a significant rotation angle, making it impractical for use on most industrial rotors because of the presence of stator vanes and rotor casings. Eulerian laser Doppler vibrometry (ELDV) is a more practical approach since the laser beam is focused at a fixed point in space while the blades under consideration sweep through the laser beam. Vibration data is therefore available for the short periods during

which each blade is exposed to the laser beam. It is the short duration of these signals that poses the main challenge associated with their signal processing, as useful results are not obtainable with the traditional frequency domain techniques.

Although there is little literature available on this subject, the application of ELDV to rotating blades has been studied since the late 1960s. Kulczyk and Davis [1] developed a laser vibrometer for this application and also noted the challenges involved with the short sample periods. They showed that ELDV samples could be analyzed for individual blade vibration frequencies above the signal fundamental frequency, and concluded that lower frequency information was more likely to represent the global response of the blades. Kulczyk and Davis [2] subsequently performed ELDV measurements on rotor blades spinning at 13000 rpm, proving the high-speed implementation capabilities of the technique. Further work ([3], [4]) was aimed at performing signal processing on individual ELDV signatures, focusing on analytically estimating low-order blade vibration frequencies. Both approaches considered pure sinusoidal blade excitation only.

Using non-harmonic Fourier analysis (NHFA), Oberholster and Heyns [5] showed that a change in the NHFA phase angle at a reference frequency is indicative of a signal frequency shift and/or a signal phase shift. Based on these findings, Oberholster and Heyns [6] implemented NHFA on a single-blade axial-flow test rotor at 720 rpm, using impulse excitation. By monitoring the phase angle trends at various blade natural frequencies, they were able to observe

deterioration in blade health from ELDV measurements. In particular they showed that maximum absolute unwrapped phase angle trends (MAUPATs) over bands around the various reference frequencies provide robust indicators of blade health deterioration. They noted however that they did not isolate the signal components as suggested by Hirata [7] because the signals were too short to accomplish this [8]. Therefore the blade health deterioration indicators they obtained were influenced by signal changes over the entire frequency bandwidth of their measurements.

This article extends the work of Oberholster and Heyns [6] to a multi-blade test rotor to verify the ability of their technique to identify damaged blades from among healthy blades. When considering a multi-blade rotor, it becomes necessary to take into account the effects of global blade vibration modes since damage on one blade affects the dynamics of the remaining blades and *vice versa*. As a result, trends may be identified from the undamaged blades which in turn may lead to the erroneous identification of damaged blades. A robust signal processing approach that accurately indicates blade damage is therefore required.

The first section of this article focuses on the experimental test setup and testing procedure. The procedure was done in two separate phases to consider damage on a single blade and damage on multiple blades consecutively. The effects on the blade-forcing frequency spectrum by blade-spacing variation due to manufacturing tolerances are studied and it is shown that these effects have to be taken into account during simulations using a finite element model (FEM).

During experimental testing, high response levels were observed in both TLDV and ELDV measurements at certain damage cases and rotor speeds, similar to those reported by Oberholster and Heyns [6]. To investigate this phenomenon, an FEM of the test rotor was constructed and subsequently the root-mean-square (RMS) values of the measurements were shown to be promising indicators of blade health.

The results obtained from signal processing on the experimental ELDV measurements at various rotor speeds ranging from 720 rpm to 1440 rpm, are discussed in the next section. It is shown that the statistical trend properties of MAUPATs as well as RMS and correlation coefficient trends are useful parameters for identifying damaged blades and monitoring the degradation in these blades. In addition, multiple ELDV measurement positions are demonstrated to be advantageous to achieving robust results. After the training of artificial neural networks (ANNs) with these parameters, it is proven that ELDV measurements can be used to accurately identify and quantify blade damage from among healthy blades.

Finally, it is verified experimentally that the first natural frequency of the individual blades can be accurately estimated from the run-up and run-down ELDV measurements.

2. Test setup

Figure 1 shows the axial-flow test rotor considered in this article. The test rotor consisted of five straight, flat blades and was driven directly by a speed-controlled motor at speeds of 720, 960, 1200 and 1440 rpm during testing. The 2 mm thick blades were attached to the rotor hub by means of clamps and had lengths and widths of 110 mm and 25 mm respectively. Due to the manufacturing tolerances of the blade-clamp interfaces, it was necessary to use epoxy to eliminate gaps between the blade and clamp surfaces prior to clamping. This was found to minimize the variation in the natural frequencies of the blades, arising from differences in the clamping boundary conditions.

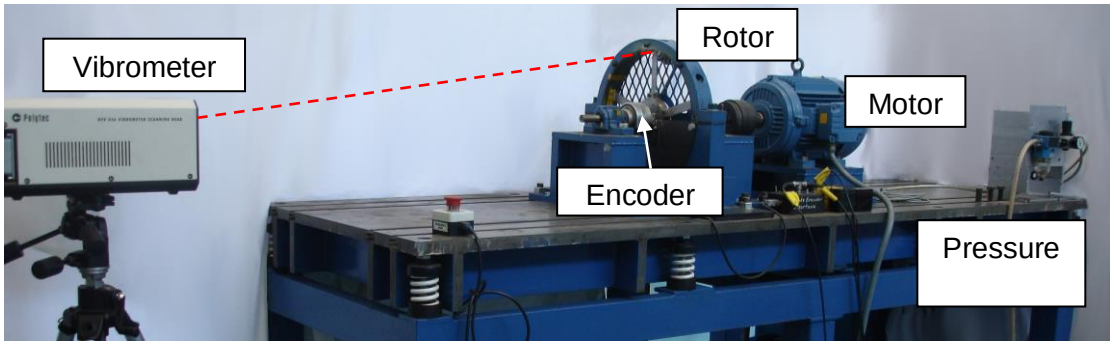

Figure 1: Test rotor

Blade excitation was accomplished by means of a stationary steady air jet, directed by a nozzle. As each blade rotated past the nozzle, the air jet impinged on the blade, resulting in impulse excitation. The nozzle was instrumented with a piezo-electric pressure sensor to measure the nozzle's back pressures during blade passage, in order to represent approximately the individual blade

excitation forces. A Heidenhain ERN 120 shaft encoder provided accurate feedback on the shaft angular position and speed, and blade TLDV and ELDV measurements were obtained with a Polytec PSV300 scanning laser vibrometer.

Prior to ELDV and TLDV testing, the natural frequencies of the individual rotor blades were obtained from stationary modal testing. Each blade was individually tested using a modal hammer as excitation and the Polytec PSV300 laser vibrometer for response measurements. This choice of excitation and measurement technique minimized any alteration in structural mass, thus ensuring accurate frequency response functions (FRFs). These FRFs were furthermore used for updating the rotor FEM.

During ELDV and TLDV testing, data acquisition and vibrometer mirror control were accomplished with LabView, using a National Instruments PCI-6110 card. The shaft encoder signal of 5000 pulses per revolution was used as a clock signal to perform position-based sampling, thus simplifying data post-processing. TLDV measurements on the test rotor were available over nearly 180^{o} as shown in Figure 2(a). Two measurement positions, namely A and B, were considered during ELDV measurements (see Figure 2(b) and Figure 2(c) respectively). At position A, the ELDV forced-vibration signature is available as the blade passes in front of the nozzle (i.e. at position A, the air impinges on the blade for the duration of each individual ELDV measurement). At position B, the blade exits the wake of the air jet, resulting in ELDV signatures that primarily consist of free vibration. The purpose of considering these two positions was

firstly to determine the sensitivity of the proposed data analysis approach to the measurement position. Secondly, it was used to investigate the possible advantages of using multiple ELDV measurement positions for online condition monitoring.

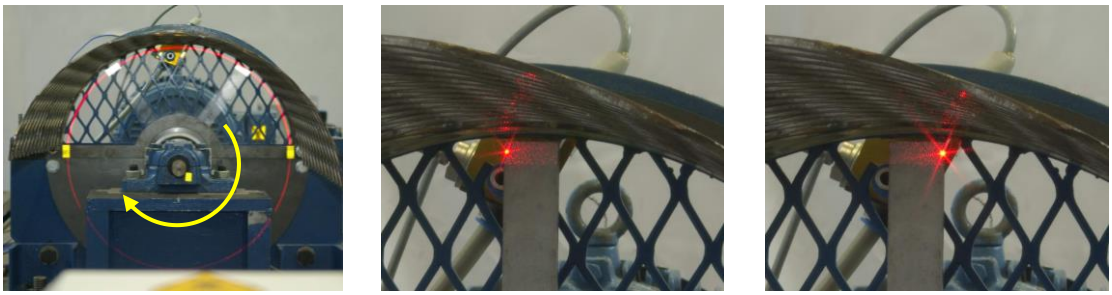

(a) (b) (c)

Figure 2: (a) TLDV implementation; (b) ELDV position A; (c) ELDV position B

Damage was simulated in various blades by increasing the depth of a slot cut in the blades' leading edges, 5 mm from the blade roots. The slots were cut with a high speed rotary tool up to a maximum depth of 16 mm and were approximately 1 mm wide. Although this was a crude approximation of actual blade damage such as cracks, it was sufficient for the demonstrative purposes of this work. Testing was conducted in two phases. During the first phase, damage was introduced on blade #1 only, whereas in the second phase, damage was considered on blade #3 and blade #5 simultaneously at different damage-increment rates. The damage cases considered are schematically depicted in Figure 3.

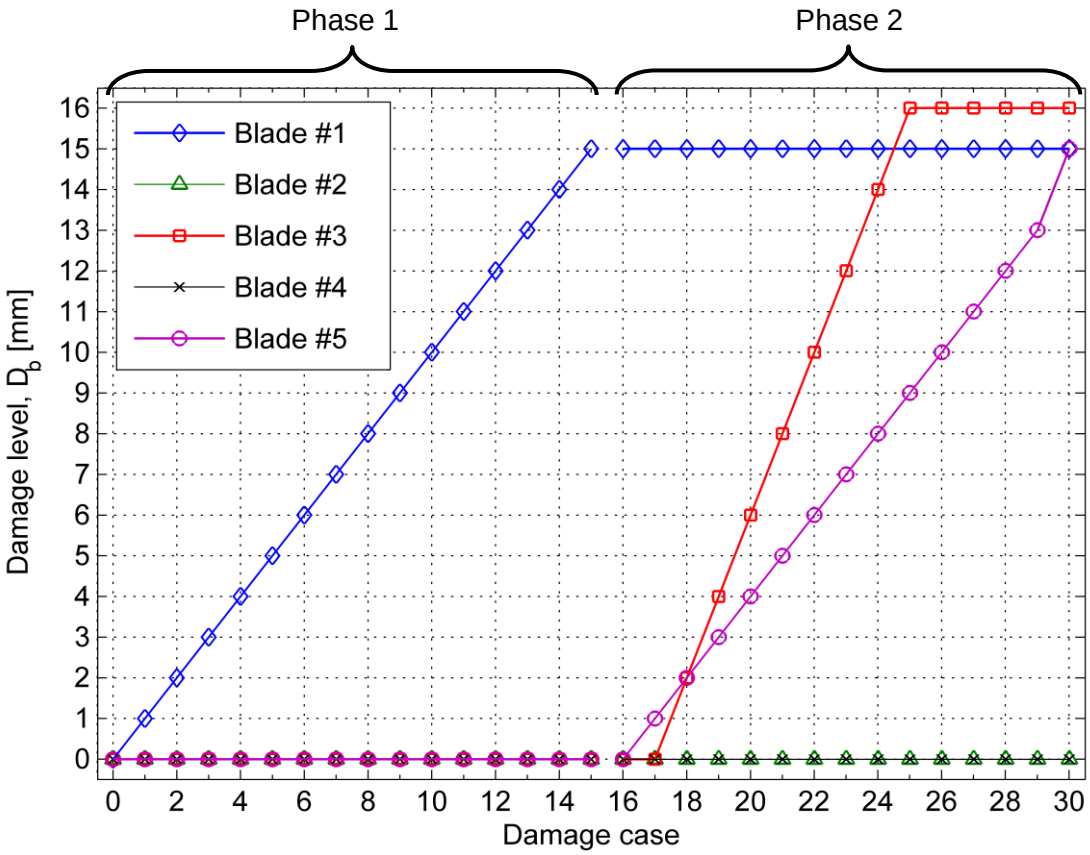

Figure 3: Damage cases considered during testing

Due to manufacturing tolerances, variation was present in the spacing of the blades in both the axial and circumferential directions. This affected the forcing frequency spectrum of the blades and in particular resulted in energy being introduced at higher rotor orders [9]. This spectrum can be estimated from the measured pressure pulses as demonstrated by the power spectral density (PSD) in Figure 4 for 720 rpm, showing the first 16 harmonics. For this reason, it was important to ensure that the relative timings between the pulse peaks used in the FEM correlated with those of the measured pressure pulses.

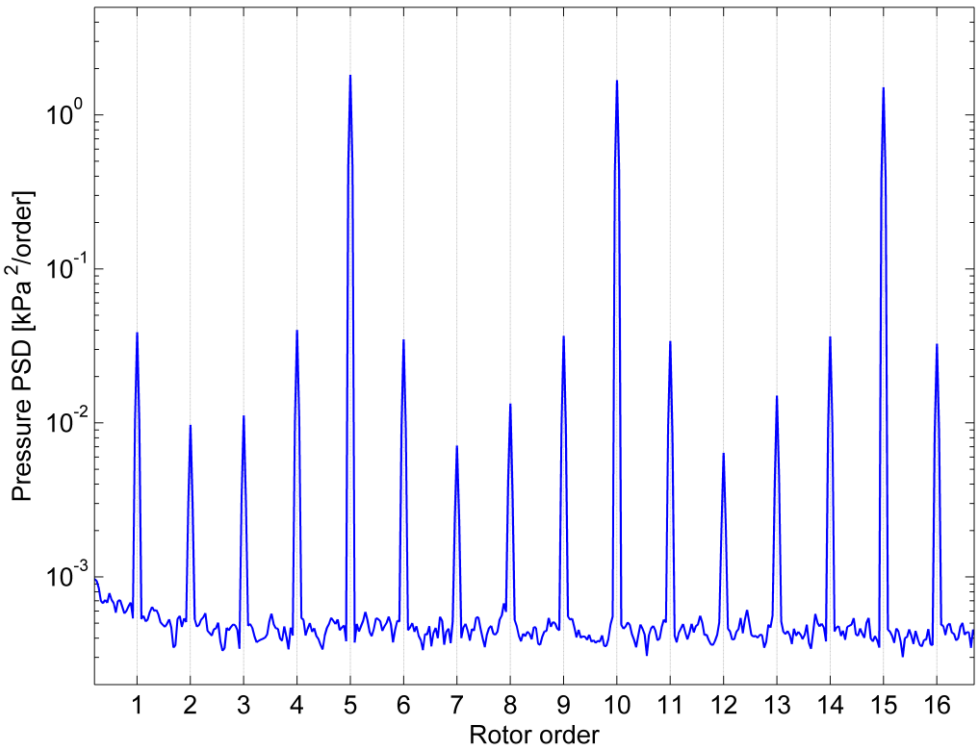

Figure 4: Pressure pulse harmonics

3. Numerical simulations

3.1. Finite element model

An FEM of the test rotor was constructed as shown in Figure 5. The blades were modelled with shell elements, whereas the hub and shaft were modelled with solid and beam elements respectively. Beam-solid and shell-solid element coupling was accomplished with multi-point constraint (MPC) elements. Damage was simulated in the model by deleting appropriate elements in the blades [6].

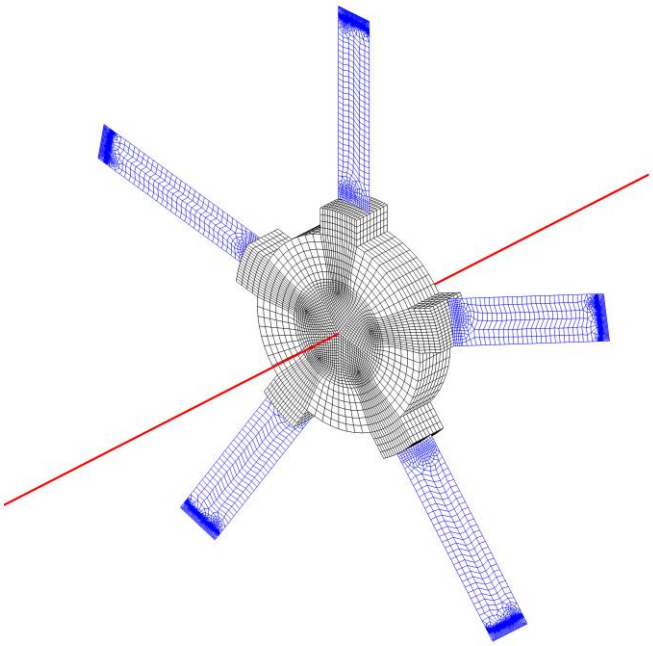

Figure 5: Finite element model

The pulses exerted on each blade by the air-jet nozzle during rotation were approximated by a concentrated force on each blade. Although it would be more representative to simulate moving loads on the blades, to do so accurately would not be trivial. The per-blade concentrated force approximation was much simpler to implement and was found to be sufficient for this work, as validated in previous work [6]. The radial locations on the blades where these forces were applied corresponded to the radial location of the nozzle (i.e. about 15 mm from the blade tips). In turn, the circumferential locations were chosen to coincide with the blade positions at which the experimental pressure pulse waveform peaks occurred. This was found to occur at about 3.6 mm from the blades'

trailing edges. Thus the locations of the simulated forces allowed the excitation of both bending and torsional modes of the blades. It was assumed that these forces were directly proportional to the respective pressure signals measured. For each blade number b, a normalized force F_b was approximated from the corresponding average pressure pulse waveform P_b:

$$F_b = k_b P_b$$

Equation 1

where k_b normalizes each P_b with respect to P_1 (i.e. the pressure pulse waveform of blade #1):

$$k_b = \frac{\max(P_b)}{\max(P_1)}$$

Equation 2

Rotational stiffening effects were included in the simulations.

3.2. TLDV simulation

TLDV was simulated in the FEM by applying F_b in succession so that the peak occurrences of each F_b corresponded with the peaks of the measured P_b signals. This is depicted in terms of rotor angle in Figure 6, with F_b obtained from P_b measured at 720 rpm. It was assumed that the F_b waveforms remained unchanged in the angular domain at the various rotor speeds and damage cases. The significant variation in the peak amplitudes of F_b shows a correlation with the variation in the blade-nozzle standoff distances measured in the test rotor blades.

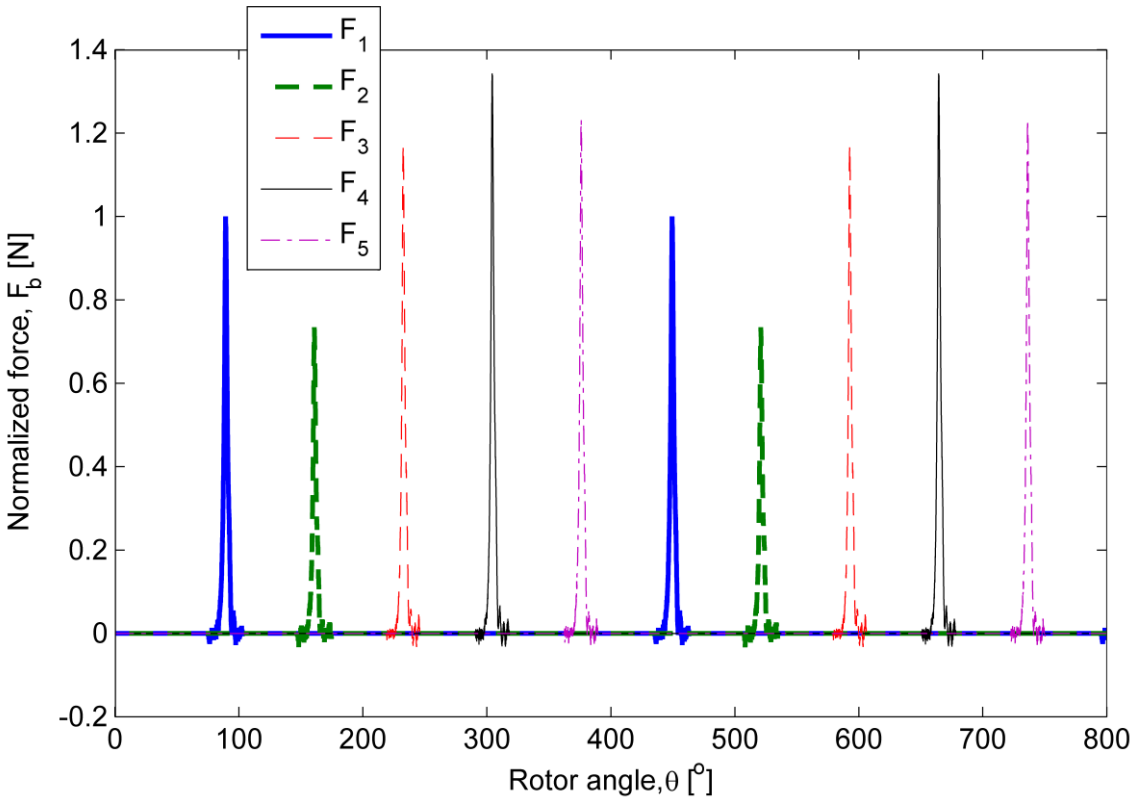

Figure 6: FEM force functions

Using initial conditions of rest, pulses were applied to the FEM over a period corresponding to 14 revolutions to allow for the development of steady-state vibration. TLDV measurements were then simulated using the FEM for the different damage levels and rotor speeds considered during the experimental testing. Figure 7 depicts a comparison of the TLDV velocity results (v_L) of numerical simulations for damage cases 0-15 with the experimental measurements for blade #1, showing a close correlation. It is observed that the numerical results lag in terms of damage level relative to the experimental results. This phenomenon is a result of experimental errors in the slot widths

and depths that occurred during the incrementation of the simulated damage levels. The damage levels simulated in the FEM were thus slight underestimations of the experimental levels, leading to the observed lag.

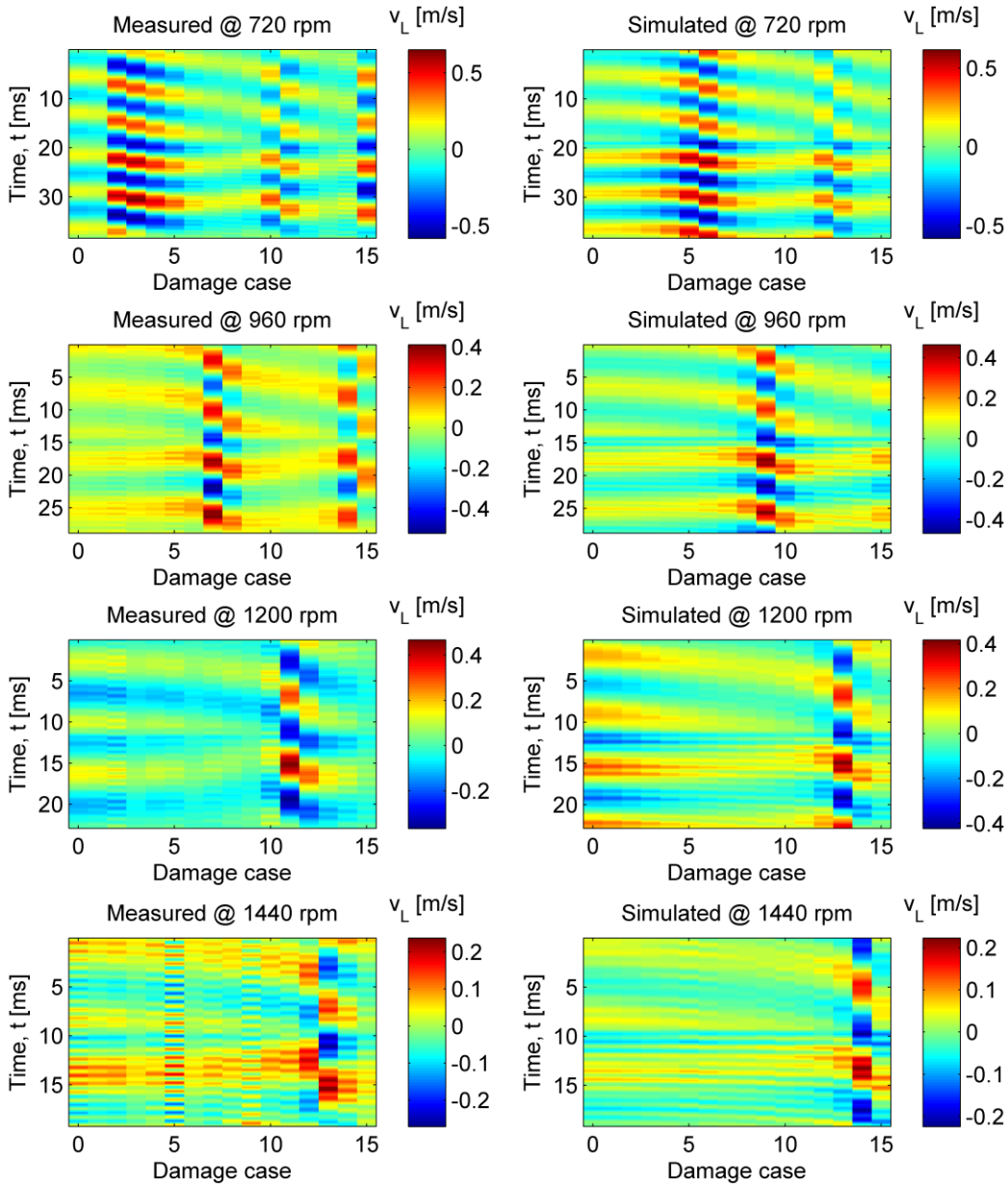

Figure 7: Time response comparison for different damage levels

At various damage cases, high response amplitudes are observed along with large phase angle changes (as can be seen from the distinct discontinuities in the velocity patterns for these damage cases), e.g. the measurements for damage cases 2, 10 and 15 at 720 rpm. This correlates with similar observations made by Oberholster and Heyns [6] for a single blade. To study this phenomenon, the change in the FEM first bending-mode natural frequency ω_1 of blade #1 with an increasing damage level is superimposed in Figure 8 on all the rotor speed orders within range. It can be seen from this figure that ω_1 coincides with rotor orders at damage levels in accordance with the discontinuities visible in Figure 7 for the simulated results.

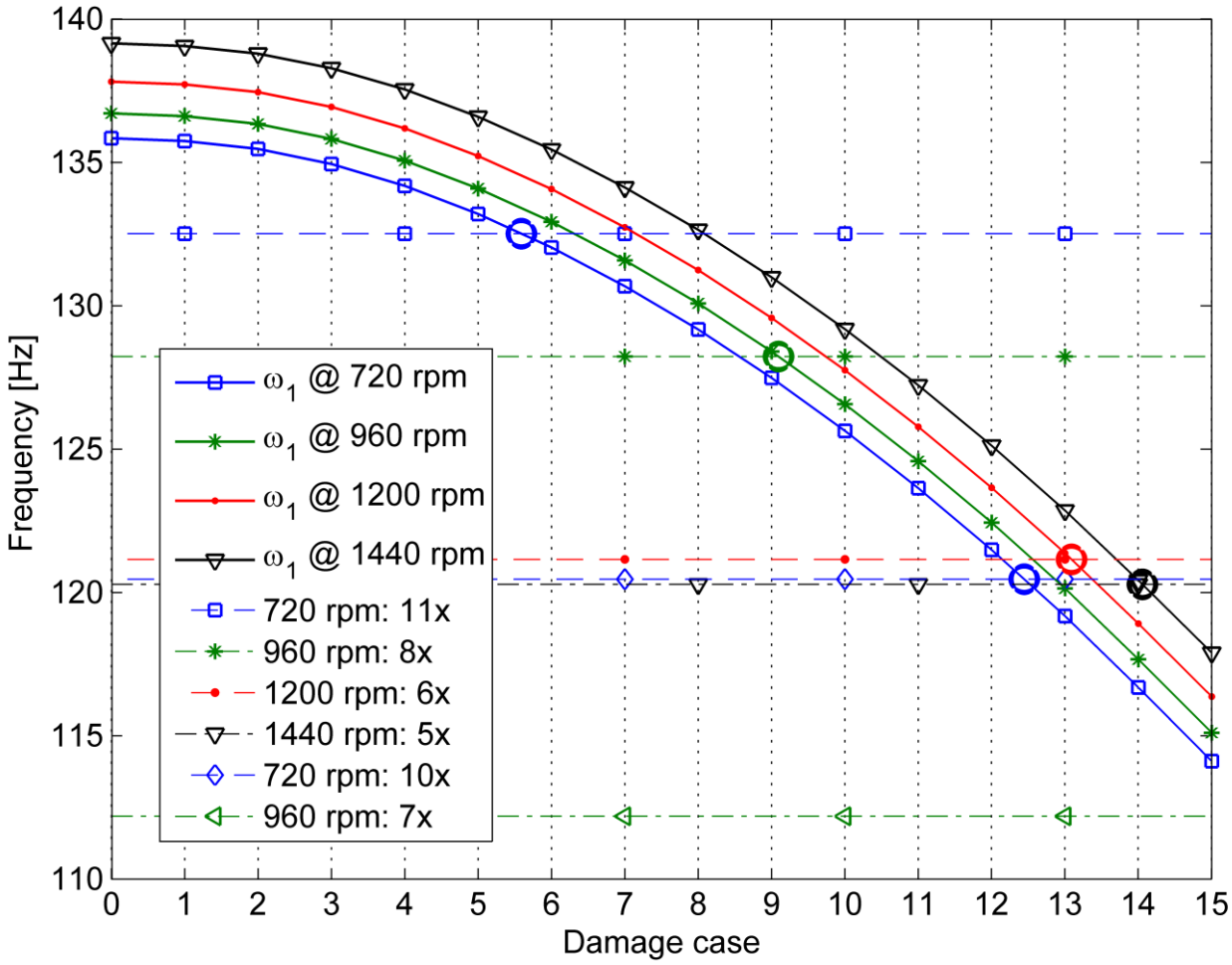

Figure 8: FEM blade #1 ω_1 comparison with rotor orders

Evaluating the velocity RMS values of the simulated results, the coinciding of high velocity response with rotor orders at the relevant damage levels is clearly demonstrated in Figure 9. It is furthermore clear from this figure that RMS holds promise as a parameter for blade condition monitoring. Not only is a systematic change in RMS value indicative of deterioration in blade health, but it can also be seen that if a sign change occurs in the RMS trend slope, ω_1 is close to a rotor order.

The latter observation however does not necessarily yield a practical on-load parameter as ω_1 can only be estimated when a blade is excited at its natural frequency. This may lead to blade failure before corrective can be taken. Nonetheless since ω_1 of each blade will inevitably coincide with a rotor order at some point during a rotor run-up or run-down, this means that ELDV records during these events are valuable for estimating individual blade ω_1 values.

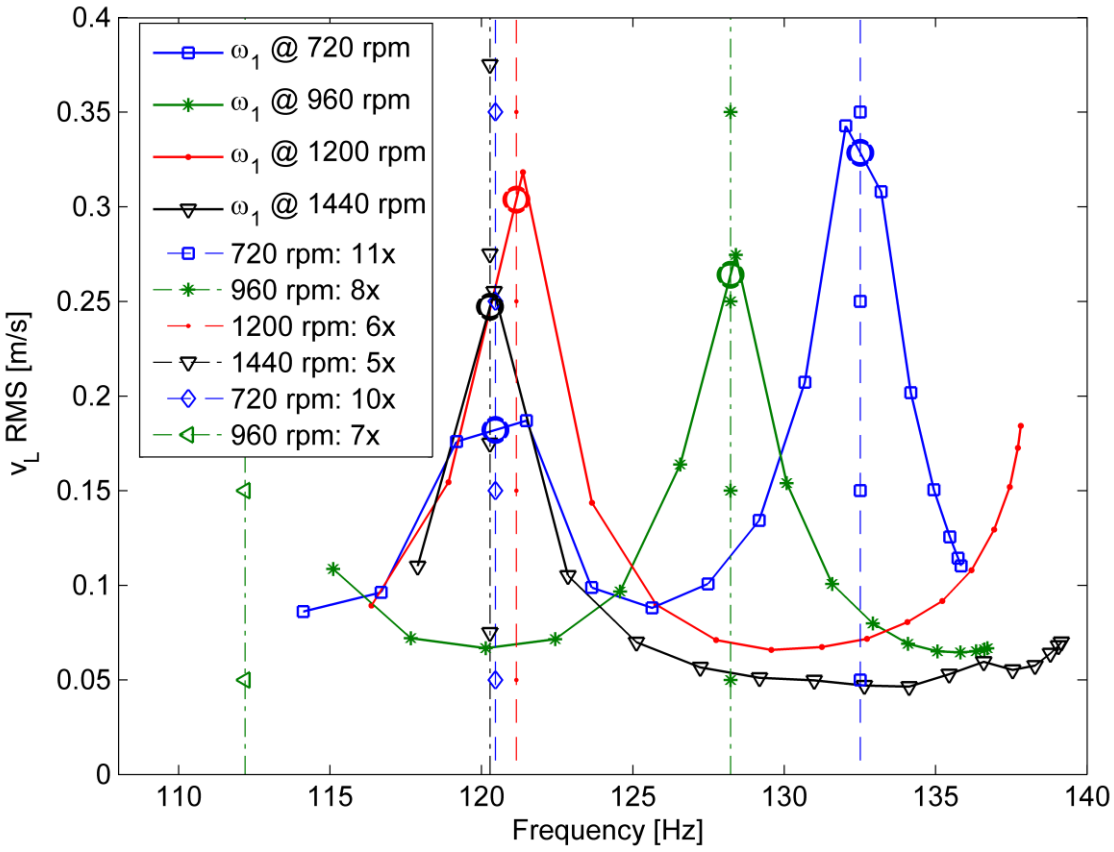

Figure 9: Blade #1 simulated RMS values as functions of FEM blade #1 ω_1

4. Experimental results

4.1. MAUPAT analysis

Oberholster and Heyns [6] performed NHFA on ELDV signals to obtain MAUPATs over ranges within 5% of the individual natural frequencies of their single blade. Since the test rotor considered in this work consisted of multiple blades, the effects of global mode shapes and blade mistuning resulted in groupings of mode shapes around various frequencies. As a result, it was decided to perform NHFA to obtain MAUPATs over ranges around the average frequencies of the various mode shape groupings. The individual ranges were determined from the variation around each reference frequency. The reference frequencies considered are listed in Table 1 along with the relevant ranges.

Table 1: MAUPAT reference frequencies

Reference number	***Reference frequency,*** f_R ***[Hz]***	***Frequency range [Hz]***
1	135	±5
2	600	±50
3	865	±25
4	1167.5	±12.5
5	2390	±50
6	3590	±20
7	4600	±40

8	6260	±30
9	7750	±150
10	9270	±50

It can readily be shown from FEM calculations that rotational stiffening result in a maximum upward shift of the natural frequencies of about 4.5 Hz at 1400 RPM. This is not significant in terms of the reference frequencies and ranges given in Table 1, and thus the frequencies of Table 1 were used for MAUPAT calculations for all the rotor speeds considered during testing. However in cases where these natural frequency shifts are substantial, it would be prudent to adjust the MAUPAT reference frequencies accordingly.

When evaluating the experimental MAUPAT results, it soon became apparent that interpreting the trends is more complicated on a multi-blade rotor than on the single-blade rotor used by Oberholster and Heyns [6]. This was expected due to the effects of global modes. Figure 10 presents the results for the MAUPATs of damage cases 0-15 around f_1. This figure shows a number of blade #1 trend jumps, corresponding with the observations from Figure 7 relating to the proximity of blade #1 ω_1 and rotor order. Secondly, it is clear that ELDV measurement position (A or B) has a definite effect on the trends. It also is evident that, depending on rotor speed and measurement position, it may prove difficult to identify the damaged blade. This is either due to the lack of a strong and consistent trend in the damaged blade MAUPATs (e.g. position A at 1440 rpm) or large changes in the MAUPATs of some undamaged blades (e.g.

position B at 960 rpm). Furthermore, the trends of blade #1 do not always increase monotonically with damage.

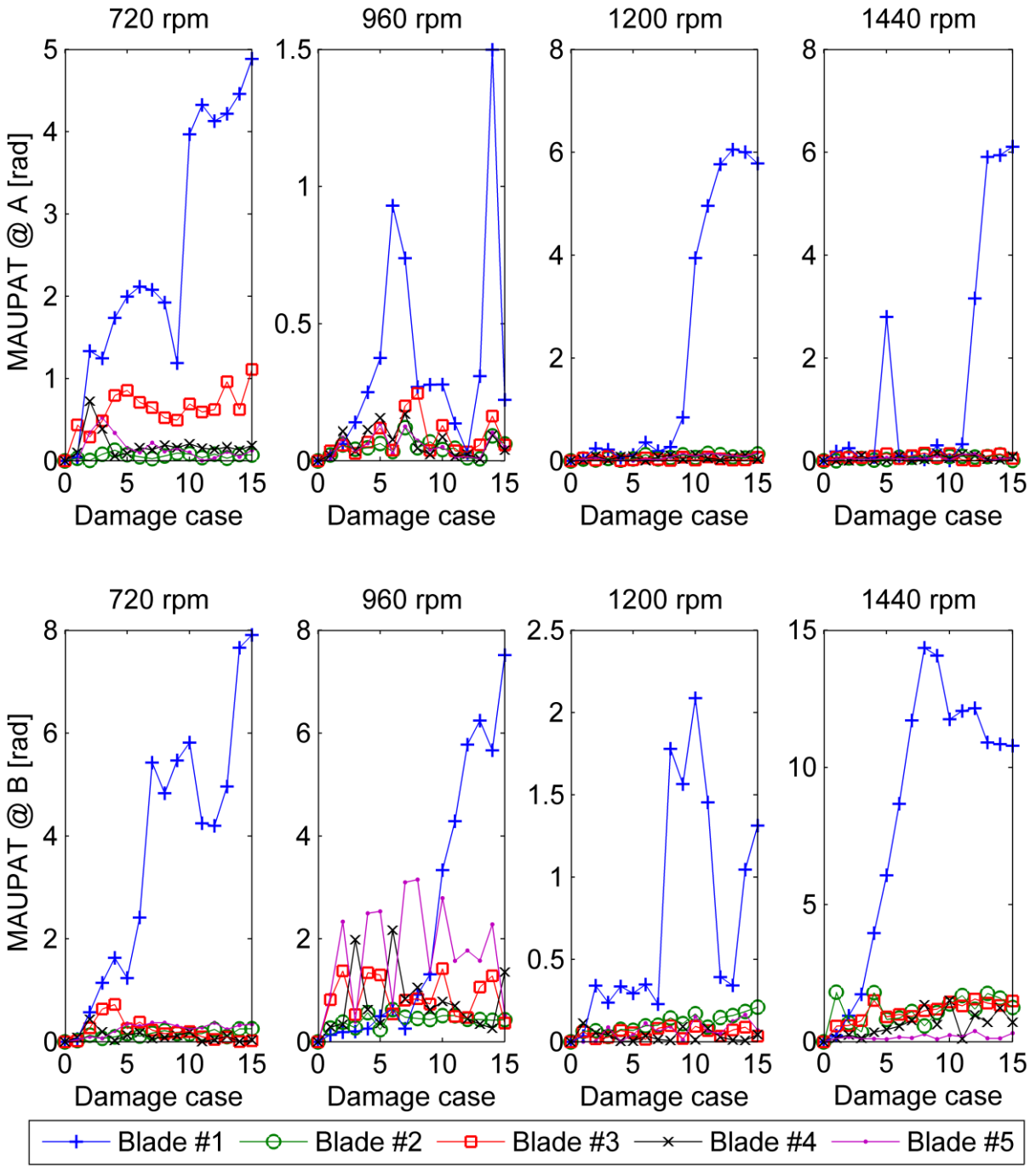

Figure 10: Damage cases 0-15 MAUPATs around f_1

In order to distinguish between damaged and undamaged blades, it was necessary to evaluate the statistical properties of the individual blade trends. After evaluating various statistical parameters, the trend standard deviation (σ) was found to yield the most favourable results. Figure 11 depicts the σ trends of the MAUPATs (σ_{MAUPAT}) around f_1, showing an improvement in trend separation in most cases. However, strong trends are still visible in undamaged blades in some cases (e.g. position B at 960 rpm).

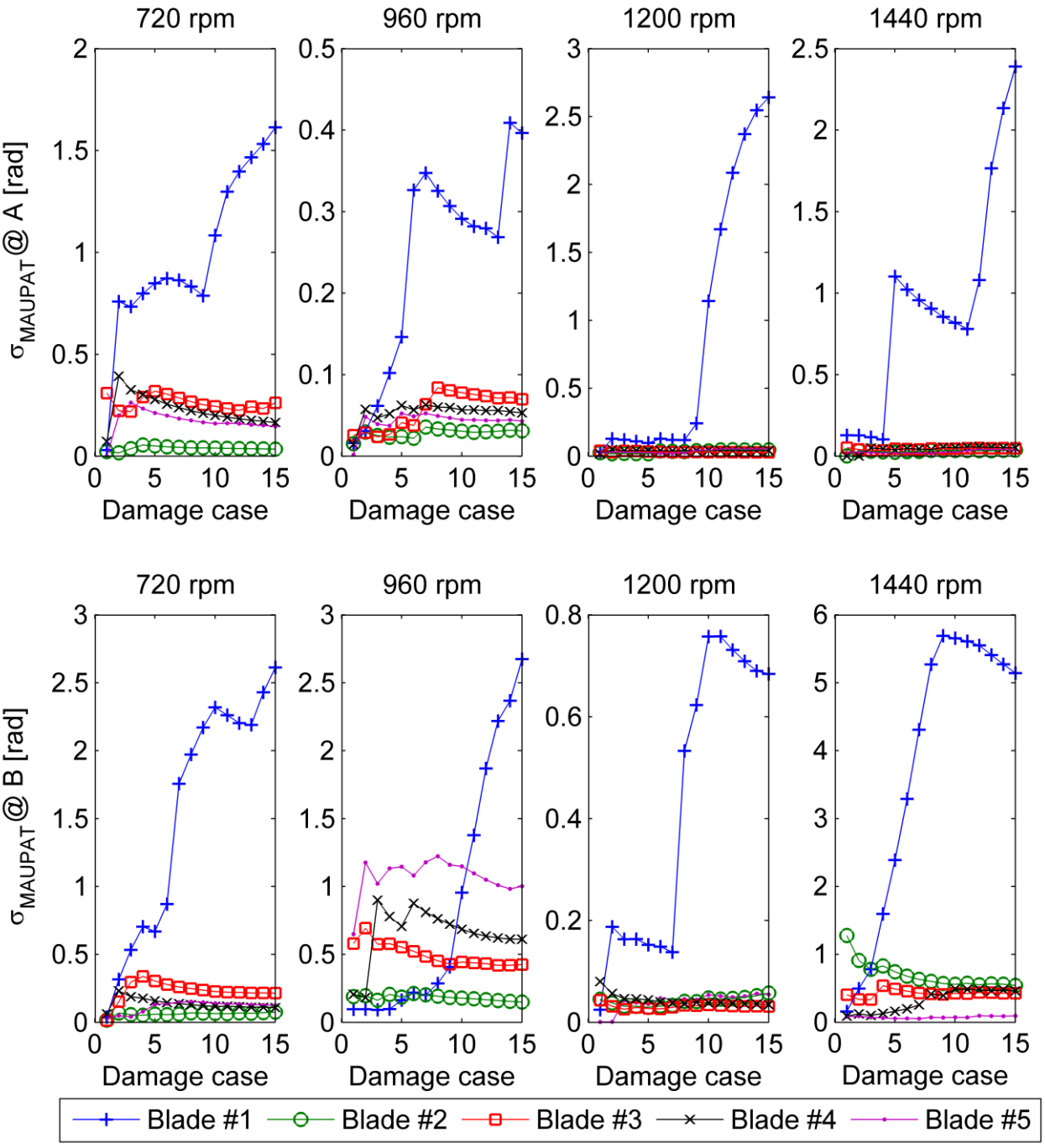

Figure 11: Damage cases 0-15 σ_{MAUPAT} trends around f_1

To obtain more robust results, the averages of the σ_{MAUPAT} trends ($\tilde{\sigma}_{MAUPAT}$) around the remaining f_R s were calculated after normalization. The outcome is

depicted in Figure 12 and it is noted that there is a definite improvement where trend separation had previously proved difficult. When this approach is taken to the measurements of damage cases 16-30, Figure 13 is obtained showing the applicability of the technique when multiple blades are damaged.

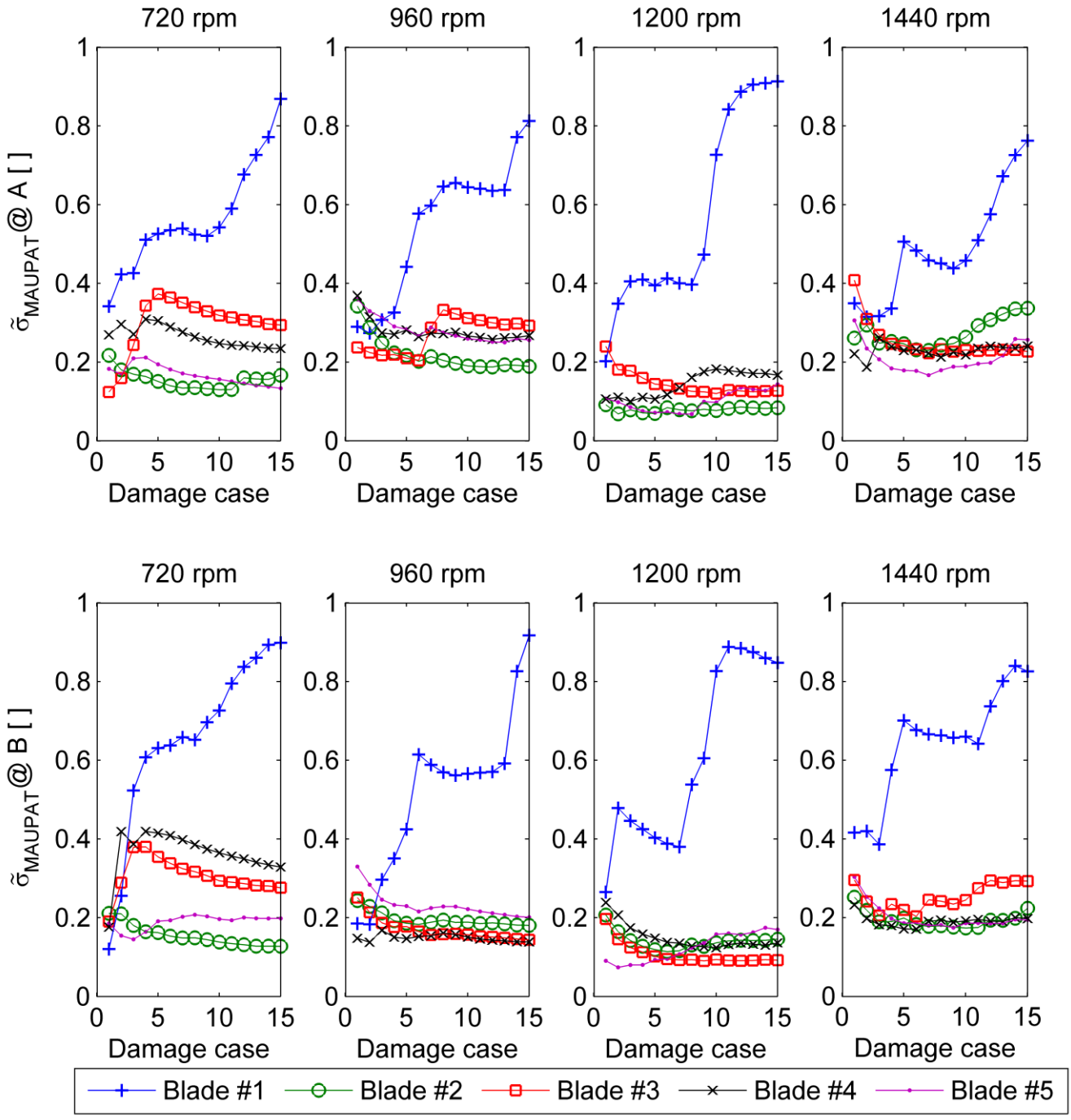

Figure 12: Damage cases 0-15 $\tilde{\sigma}_{MAUPAT}$ trends

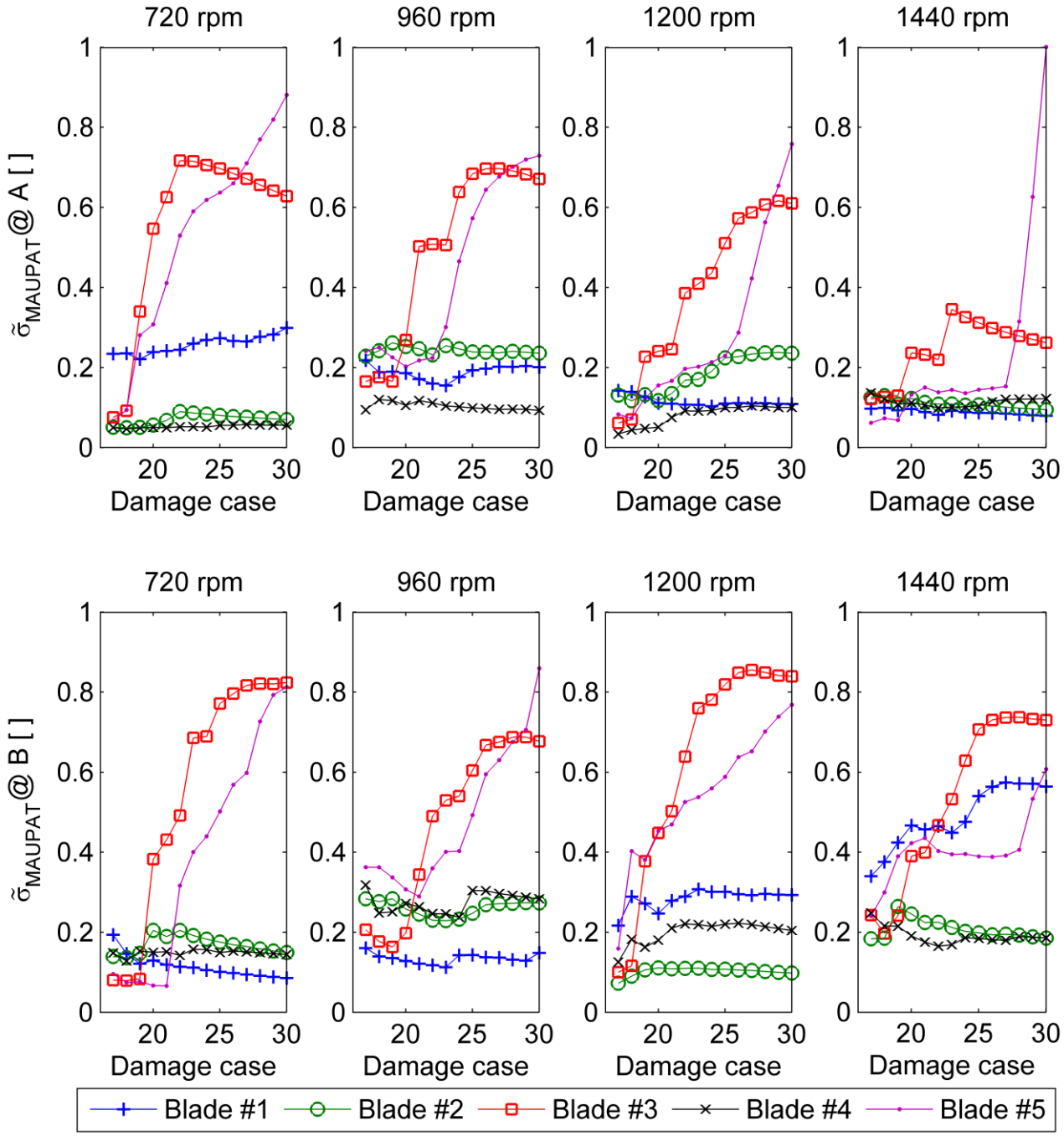

Figure 13: Damage cases 16-30 $\tilde{\sigma}_{MAUPAT}$ trends

Finite-duration impulse response (FIR) filtering and Vold-Kalman filtering were applied to the signals in order to investigate whether a further improvement in

the trends could be obtained via frequency component isolation prior to NHFA analysis. No significant improvement was obtained in the results, however.

4.2. Time domain

Various time domain parameters were evaluated, namely crest factor, kurtosis, variance, covariance, correlation coefficient, RMS and skewness [10]. Of these, the RMS and correlation coefficient yielded the best results. Figure 14 and Figure 15 depict the RMS standard deviation trends (σ_{RMS}) for damage cases 0-15 and those for damage cases 16-30 respectively. In general, good results were obtained for all the damage cases except for the lower damage cases at position A at 960 rpm and 1200 rpm. The σ_{RMS} results obtained at position B at 720 rpm for blade #5 erroneously show a strong trend for damage cases 0-15 (Figure 14). As seen from Figure 15, trend separation at both measurement locations is poor at 1440 rpm for damage cases 16-28.

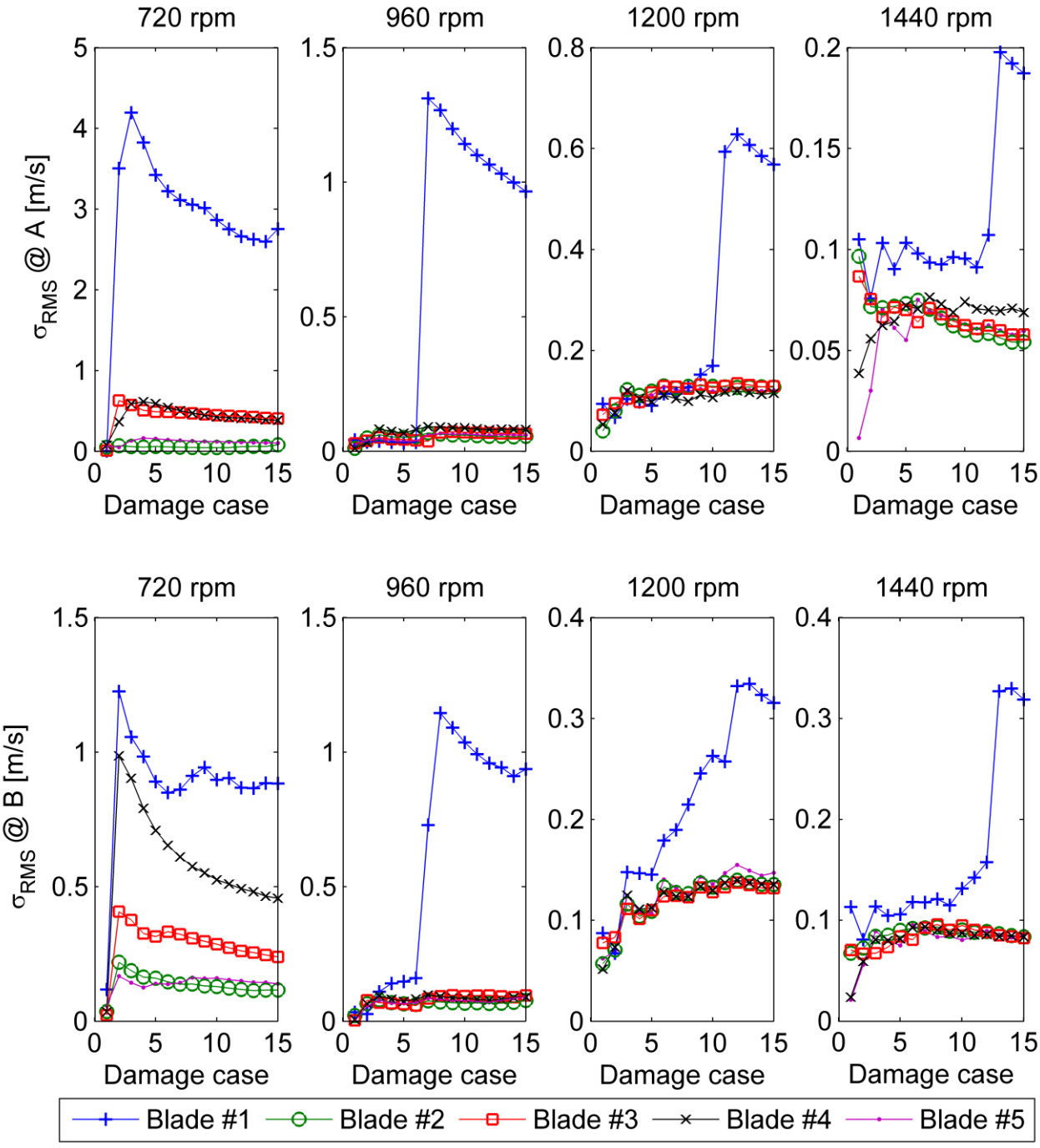

Figure 14: Damage cases 0-15 σ_{RMS} trends

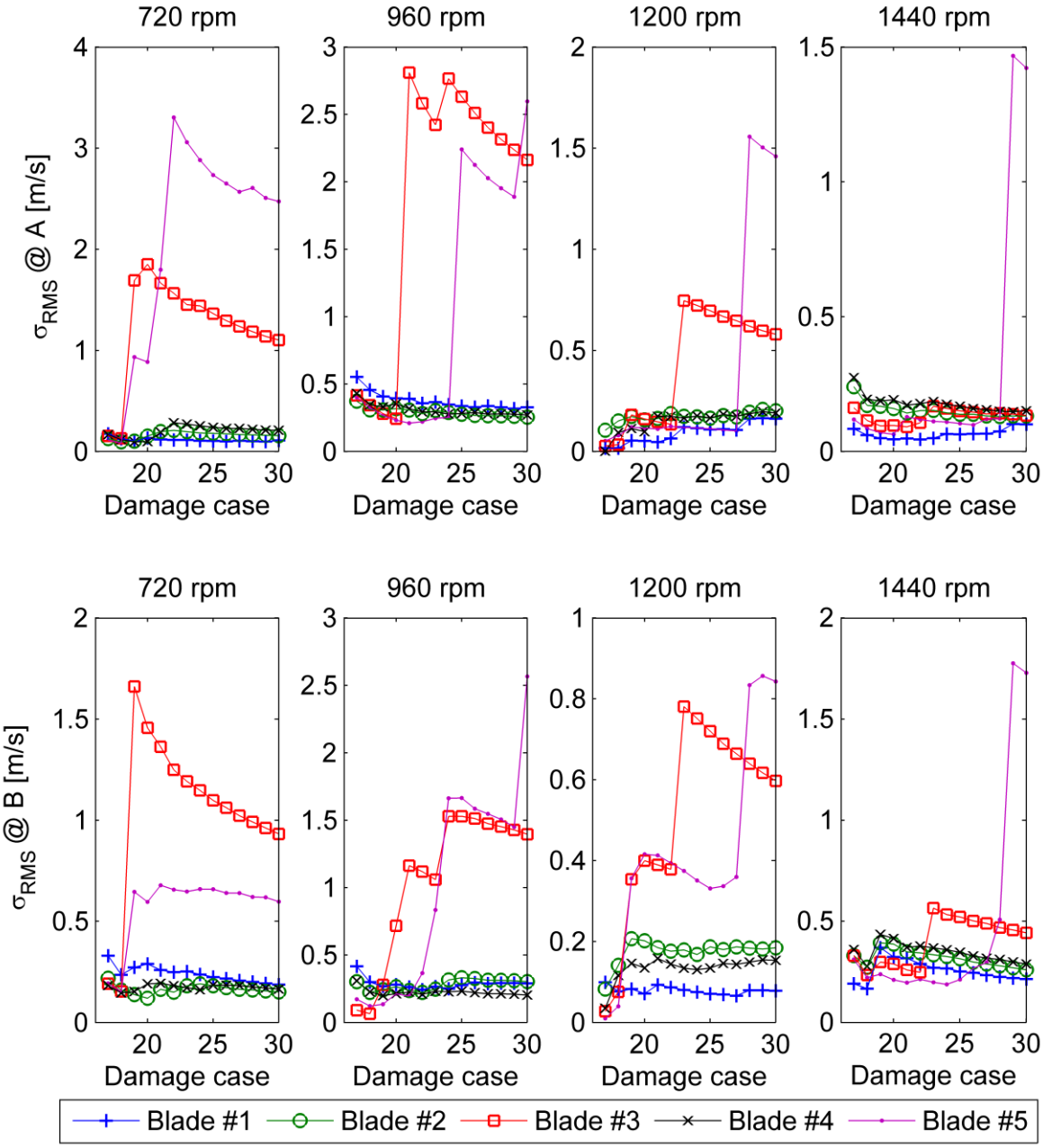

Figure 15: Damage cases 16-30 σ_{RMS} trends

The trends of correlation coefficient standard deviation (σ_{CORR}) are considered in Figure 16 and Figure 17 for damage cases 0-15 and 16-30 respectively. Once again, good results are generally obtained for all damage cases. An

erroneous trend is visible for damage cases 0-15 for blade #3 at position A at 720 rpm (Figure 16). Blade #4 also exhibits strong trends at 720 rpm at both measurement locations for damage cases 0-15. Figure 17 indicates that good results are obtained at position A whereas weak trends are visible for blade #5 at position B except at 1200 rpm. However, at position B, a strong σ_{CORR} trend for blade #4 is erroneously indicated at 1200 rpm. Also at both measurement locations, strong erroneous trends for blade #2 are visible at 720 rpm.

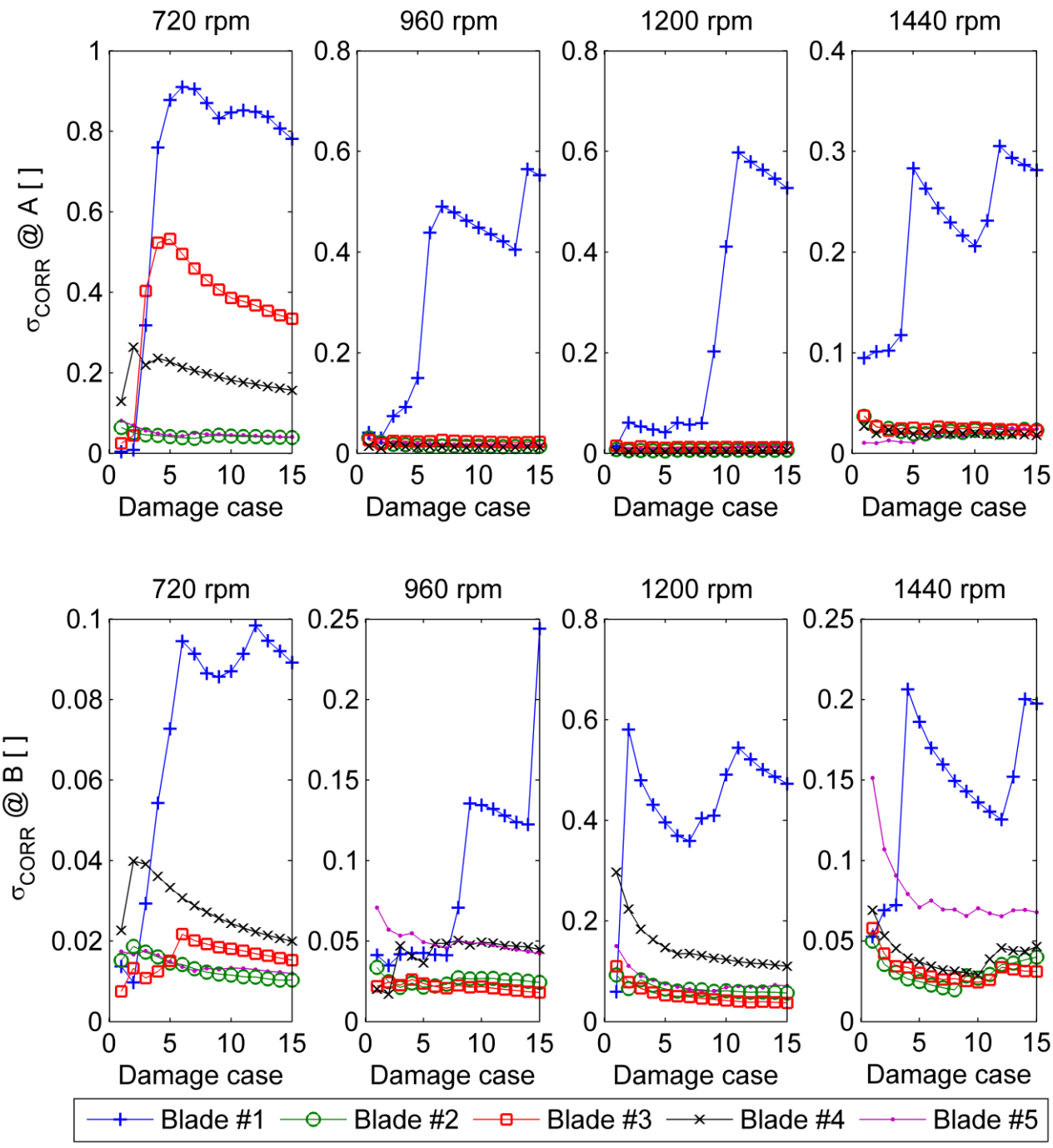

Figure 16: Damage cases 0-15 σ_{CORR} trends

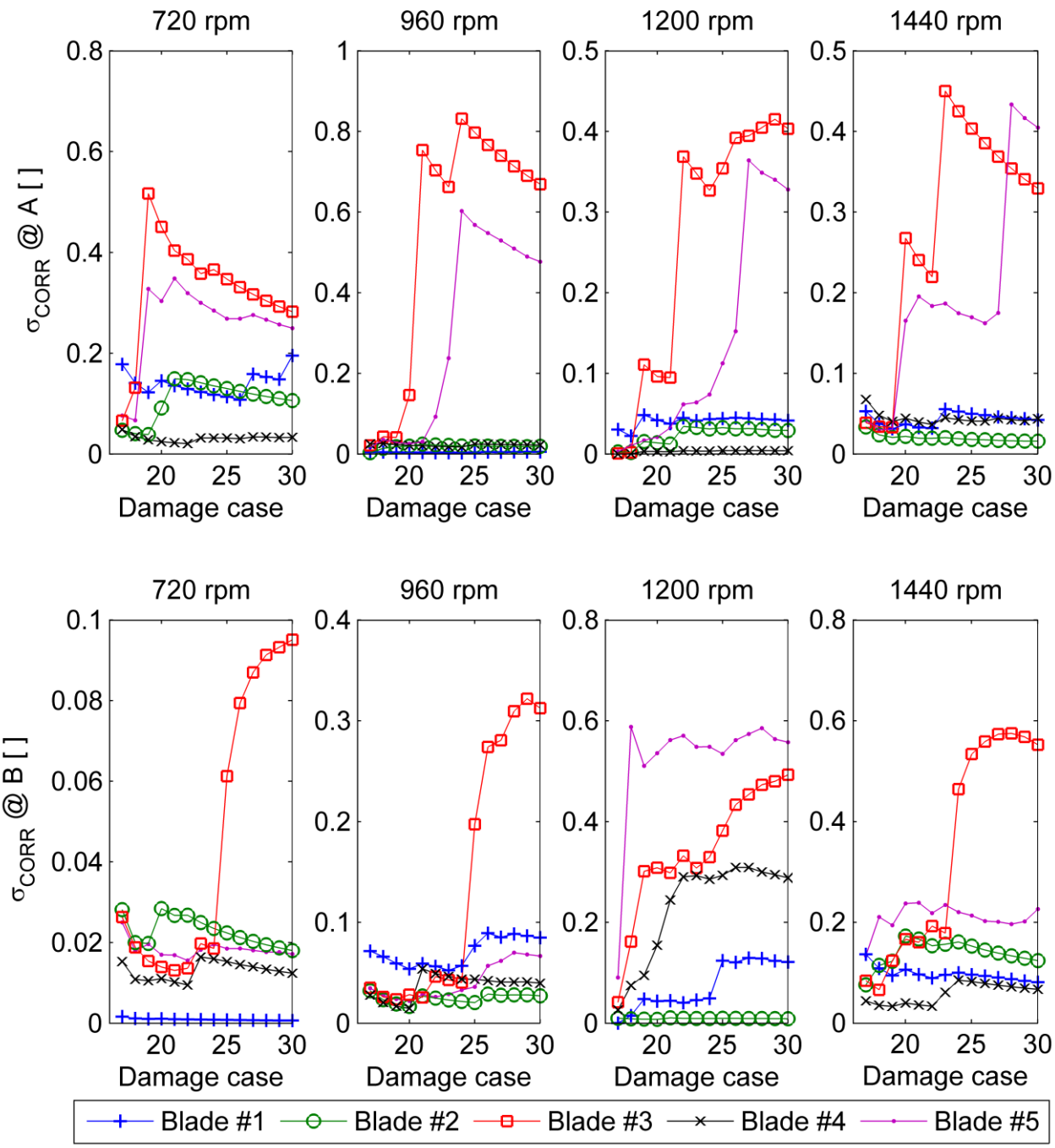

Figure 17: Damage cases 16-30 σ_{CORR} trends

4.3. ANN implementation

It is evident from the results obtained for $\tilde{\sigma}_{MAUPAT}$, σ_{RMS} and σ_{CORR} that the different parameters need to be considered in conjunction to identify and quantify blade damage accurately. In addition, it is clear that the parameters from multiple ELDV measurement positions are advantageous to this purpose. One approach to efficiently harvesting the information from the diverse parameters is to employ ANNs.

Using an architecture consisting of two layers, one with 14 neurons and the other with a single neuron, a separate ANN was trained for each rotor speed. Tan-Sigmoid transfer functions were used for all the neurons.

Ten different sets of parameters were extracted for each blade from the average of ten ELDV samples for each damage case and rotor speed. Each set consisted of seven parameters, namely $\tilde{\sigma}_{MAUPAT}$ at position A and B, σ_{RMS} at position A and B, σ_{CORR} at position A and B as well as the blade number b. Each network was then trained to yield the blade-specific damage level D_b. A schematic diagram of the ANN architecture is presented in Figure 18.

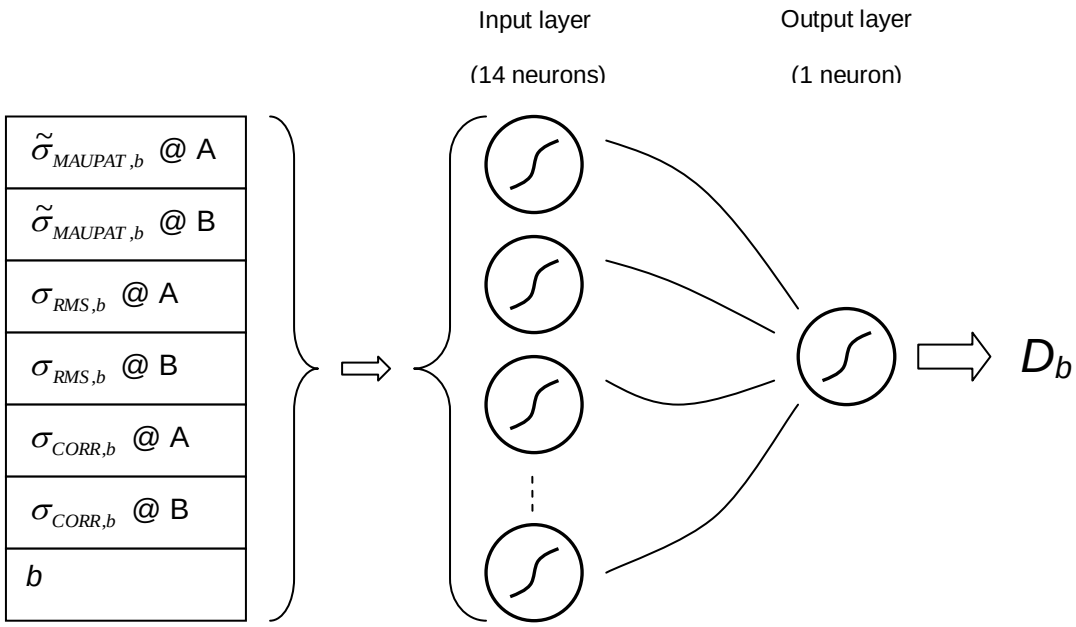

Figure 18: ANN architecture

Following training with eight sets of parameters, each ANN was evaluated with the two remaining sets and the average results are depicted in Figure 19 with the dashed lines representing the ANN training targets. Good results are observed in this figure, showing the ANNs to be capable of both identifying and quantifying blade damage.

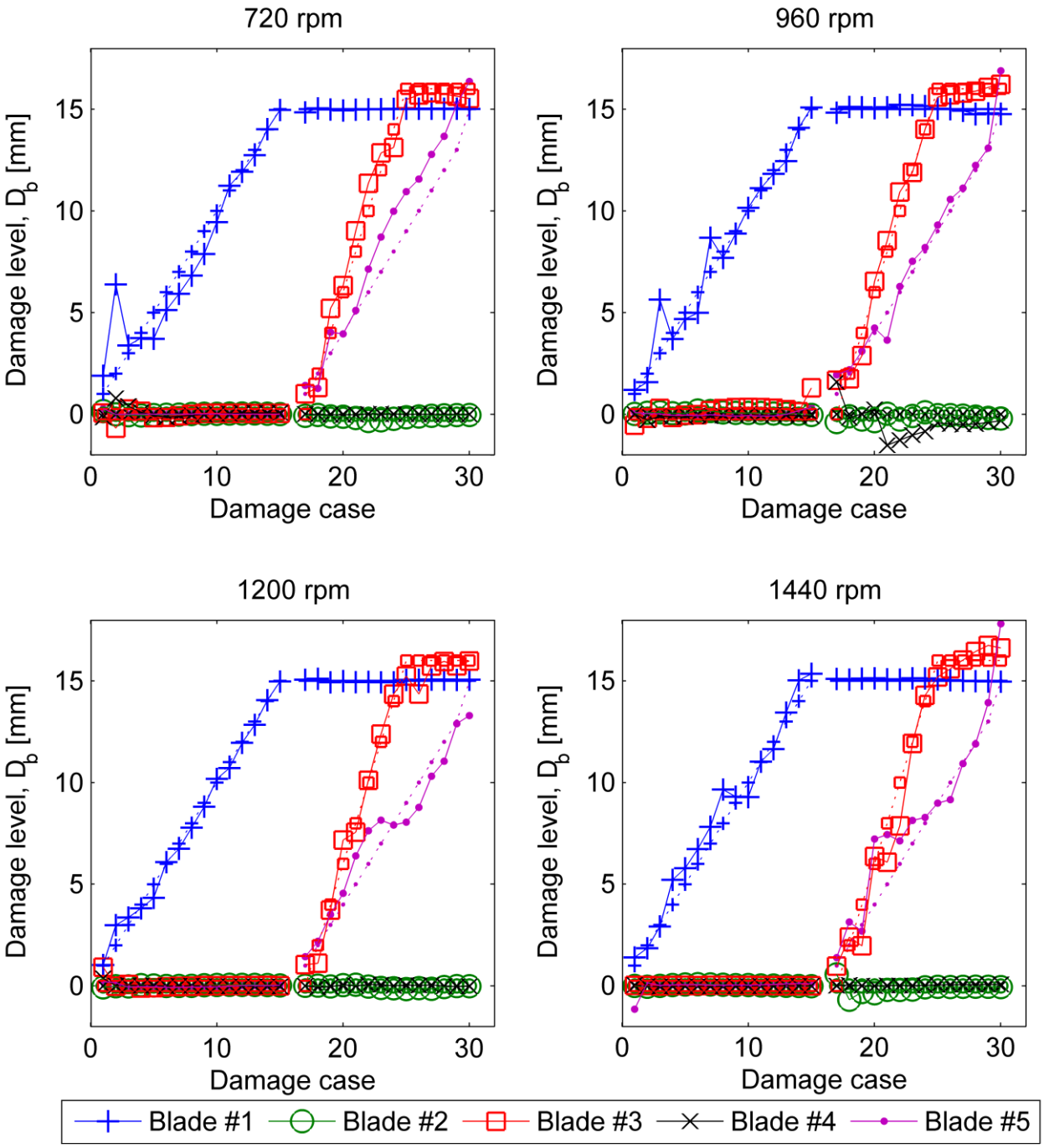

Figure 19: ANN results

To implement such ANNs in an industrial environment, it will be necessary to build up a library of likely damage scenarios for ANN training purposes. This

can be done cost efficiently by using numerical results to train the ANNs and then implement the ANNs on experimental data as demonstrated by Oberholster and Heyns [11].

4.4. Natural frequency estimation

The results presented in paragraph 4.1 to 4.3 are useful for identifying and quantifying blade damage relative to a reference point. In order to obtain that reference point, it would be most useful to know the natural frequencies of each individual blade. Although these frequencies can be obtained via offline FRF testing, this approach requires long downtimes and can typically be performed only during outages. It is therefore desirable to estimate the frequencies in an online fashion.

In paragraph 3.2 it was shown numerically that ω_1 can be estimated for each blade from run-up and run-down ELDV records. To validate this, ELDV measurements were taken on the test rotor at position A during the run-up and run-down events over rotor speeds ranging from 340 rpm to 1440 rpm. The RMS trend of the ELDV run-down signatures of blade #1 at position A is given in Figure 20 for damage case 30, showing a number of peaks.

Consider a vector $\overline{\psi}$ containing the rotational frequencies Ω in descending order at the predominant peaks:

$$\overline{\psi} = [\Omega_1, \Omega_2, ..., \Omega_q]$$

Equation 3

with $\Omega_1 > \Omega_2 > ... > \Omega_q$ and q is the number of peaks considered.

Assuming that the first natural frequency (ω_1) of each blade remains largely unchanged during a rotor run-up or run-down, and since it can be assumed that an RMS peak occurs when one of the rotor speed order frequencies is close to the relevant blade's ω_1, the order number of the pertinent Ω has to be incrementally larger than the order number corresponding to the preceding RMS peak and Ω. Thus if a vector $\bar{\varepsilon}$ consisting of the rotor order numbers at the RMS peaks is defined as

$$\bar{\varepsilon} = \delta + [1, 2, ..., \mathrm{q}]$$

Equation 4

with δ an integer constant, a vector $\bar{\omega}$ can be constructed with elements approximating ω_1 by multiplying the elements of $\bar{\psi}$ and $\bar{\varepsilon}$:

$$\bar{\omega} = \left[\bar{\varepsilon}_1\bar{\psi}_1,\ \bar{\varepsilon}_2\bar{\psi}_2,\ ...,\ \bar{\varepsilon}_\mathrm{q}\bar{\psi}_q\right]$$

Equation 5

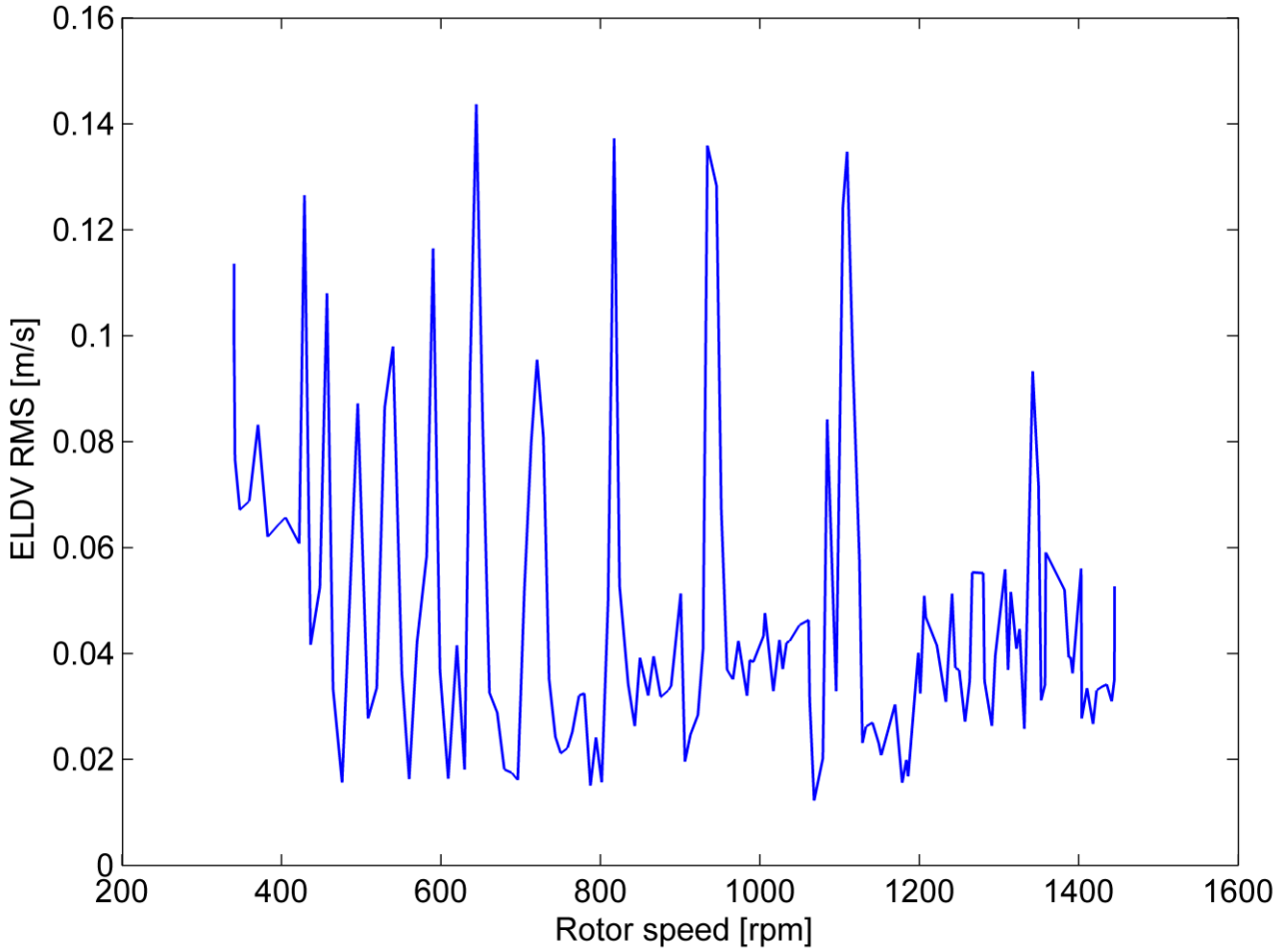

Figure 20: Blade #1 run-down ELDV RMS signature

By selecting δ so that the standard deviation of $\overline{\omega}$ is minimized, an estimate of ω_1 can be obtained from the mean of $\overline{\omega}$:

$$\omega_{1,est} = \frac{\overline{\varepsilon} \cdot \overline{\psi}}{q}$$

Equation 6

Using the experimental results from both a run-up and run-down signature, the average $\omega_{1,est}$ results are listed in Table 2, showing a good correlation with the natural frequencies obtained from modal testing on the stationary rotor.

Blade number, b	***FRF frequency [Hz]***	$\omega_{1,est}$ ***[Hz]***	***% error***
1	106.25	109.48	3.04
2	137.5	138.11	0.44
3	103.125	105.04	1.89
4	137.5	138.34	0.61
5	109.375	111.64	2.07

Table 2: Natural frequency estimation

If the machine is operated in such a way that run-up and run-down events occur regularly, $\omega_{1,est}$ can be used as an additional ANN parameter.

When high rotor speeds are considered (i.e. rotational phenomena such as centrifugal stiffening influence ω_1 significantly), it will be necessary to include a correction component in Equation 6:

$$\omega_{1,est} = \frac{\bar{\varepsilon} \cdot \bar{\psi} - \bar{\lambda}}{q}$$

Equation 7

with $\bar{\lambda} = [\lambda_1, \quad \lambda_2, \quad ..., \quad \lambda_q]$ a vector expressing the shift in ω_1 at each Ω due to rotational effects. The values of $\bar{\lambda}$ can be obtained from appropriate numerical analysis.

5. Conclusions

In this article it has been shown that ELDV is viable as an online blade condition monitoring tool for multi-blade rotors. Employing both NHFA and time domain analysis on ELDV measurements from a test rotor at two different measurement positions, the parameters yielded were successfully used to train ANNs for the purpose of identifying and quantifying blade deterioration.

It is demonstrated both numerically and experimentally that run-up and run-down ELDV signatures are valuable in approximating the first bending natural frequencies of individual blades and can serve as an additional condition monitoring parameter.

Further work is under way for implementing on industrial rotors the proposed condition monitoring approach. In terms of the ELDV measurement technique, the practical issues that will have to be addressed include blade reflectivity and the use of optical fibres for laser beam transmission. Alternative sensors are also being investigated. With regards to the signal processing approach, the effect of blade loading conditions and other operational variables on the results should also be taken into account.

Although the damage simulation approach used in this work was a crude approximation of actual blade cracks, it was sufficient to demonstrate the proposed condition monitoring approach. Nonetheless, actual cracks do introduce additional structural complexities such as nonlinear stiffness, and as a result further work is necessary to validate the condition monitoring approach for true blade damage scenarios.

References

[1] W.K. Kulczyk, Q.V. Davis, Laser measurements of vibrations on rotating objects, *Optical and Quantum Electronics* 2(3) (1970) 177-179.

[2] W.K. Kulczyk, Q.V. Davis, Laser Doppler instrument for measurement of vibration of moving turbine blades, *Proceedings of the Institution of Electrical Engineers* 120(9) (1973) 1017-1023.

[3] R.A. Cookson, P. Bandyopadhyay, Fiber-optic laser-doppler probe for vibration analysis of rotating machines, *Journal of Engineering for Power* 102(3) (1980) 607-612.

[4] A.K. Reinhardt, J.R. Kadambi and R.D. Quinn, Laser vibrometry measurements of rotating blade vibrations, *Journal of Engineering for Gas Turbines and Power* 117(3) (1995) 484-488. (DOI: 10.1115/1.2814121)

[5] A.J. Oberholster and P.S. Heyns, A study of the non-harmonic Fourier analysis technique, *Proceedings of the 21st International Congress on Condition Monitoring and Diagnostic Engineering Management*, Prague, Czech Republic, 2008, pp. 361-370.

[6] A.J. Oberholster and P.S. Heyns, Online condition monitoring of axial-flow turbomachinery blades using rotor-axial Eulerian laser Doppler vibrometry, *Mechanical Systems and Signal Processing* 23 (2009) 1634-1643. (DOI: 10.1016/j.ymssp.2009.01.001)

[7] Y. Hirata, Non-harmonic Fourier analysis available for detecting very low-frequency components, *Journal of Sound and Vibration* 287(3) (2005) 611-613. (DOI: 10.1016/j.jsv.2005.01.025)

[8] T. Muraoka, Y. Nishioka, Separation of adjacent frequency components in generalized harmonic analysis (GHA), *The 47th Midwest Symposium on Circuits and Systems 2* (2004) pp. II-157 - II-160. (DOI: 10.1109/MWSCAS.2004.1354115)

[9] D. Ewald, A. Pavlovic and J.G. Bollinger, Noise reduction by applying modulation principles, *The Journal of the Acoustical Society of America* 49(5A) (1971) 1381-1385. (DOI: 10.1121/1.1912513)

[10] M.P. Norton and D.G. Karczub, *Fundamentals of noise and vibration analysis for engineers*, Cambridge, UK: Cambridge University Press, 2003.

[11] A.J. Oberholster and P.S. Heyns, On-line fan blade damage detection using neural networks, *Mechanical Systems and Signal Processing* 20 (2006). (DOI: 10.1016/j.ymssp.2004.09.007)

Captions

Figures

Tables